Applied Catalysis B: Environmental 280 (2021) 119374

Contents lists available at ScienceDirect

Applied Catalysis B: Environmental

journal homepage: www.elsevier.com/locate/apcatb

Unraveling the origin of extraordinary lean NOx reduction by CO over Ir-Ru bimetallic catalyst at low temperature

Young-Woo You[a,b,1], Young Jin Kim[a,1], Jin Hee Lee[a], Malik Waqar Arshad[a,c], Seok Ki Kim[a], Soo Min Kim[a], Hyunjoo Lee[b], Levi T. Thompson[d], Iljeong Heo[a,*]

[a] Chemical & Process Technology Division, Korea Research Institute of Chemical Technology, Daejeon 34114, Republic of Korea
[b] Department of Chemical and Biomolecular Engineering, Korea Advanced Institute of Science and Technology, Daejeon 34141, Republic of Korea
[c] Advanced Materials and Chemical Engineering Technology, University of Science & Technology, Daejeon 34113, Republic of Korea
[d] Chemical & Biomolecular Engineering, University of Delaware, Newark, DE 19716, United States

ARTICLE INFO

Keywords:
Lean NOx reduction
CO-NO-O_2 reaction
Iridium-Ruthenium alloy
NO dissociation
Surface oxygen

ABSTRACT

Ir-Ru/Al_2O_3 developed has shown an outstanding activity for reducing NOx by CO at low temperature in excess oxygen. However, it has remained elusive how the Ir-Ru catalyst derives this unique reactivity. Here, we tried to unveil the origin of the synergistic effect in the Ir-Ru catalyst on the lean deNOx by CO. Ir-Ru/Al_2O_3 showed superb NOx reduction activity along with high N_2 selectivity compared to monometallic catalysts. Results of EXAFS and XRD studies indicated the formation of Ir-Ru alloy phases on the alumina. These alloy phases were likely to accelerate reaction steps required for the NOx reduction by CO, based on temperature programmed experiments together with DFT calculations. Ir-Ru/Al_2O_3 appeared to effectively dissociate NO on the bimetallic site, which could successively be reutilized by the facile CO-O reaction, believed to be the primary causes for the excellent deNOx activity of Ir-Ru/Al_2O_3 by CO under lean exhaust condition.

1. Introduction

Anthropogenic emissions of greenhouse and toxic gases by burning fossil fuels have become a world-wide issue with global climate change and air pollution during the past several decades. Knowing that transport is one of the primary source of these gases, considerable efforts have been devoted to regulating vehicle emissions along with a fuel economy. However, internal combustion engines are still necessary in the powertrain of the automobiles because of issues of cost and infrastructure required for next generation vehicles which do not use fossil fuels directly for propulsion. In this aspect, diesel engine technology may be highly attractive in terms of CO_2 mitigation, since it fundamentally operates at higher efficiency than its gasoline counterpart. In fact, the fleet average CO_2 emissions of new passenger cars in EU, which had decreased monotonously for roughly a decade, rebounded from 2017, possibly due to the decrease of the diesel market share together with a shift of consumer preference toward sport utility vehicles (SUVs) [1]. Similarly, lean-burn gasoline engines would provide another way of improving fuel economy. However, those highly efficient combustion technologies have been basically suffering from the emission of NOx in oxygen rich operation.

Selective catalytic reduction of NOx by urea (urea-SCR) has been commonly recognized as one of the most reliable ways of reducing NOx in an oxygen rich condition owing to its high activity and durability, which has been carried out to satisfy strengthened exhaust emission regulations [2]. However, urea-SCR still has some drawbacks such as high cost, complexity of the system, and periodical refill of urea solution by users [3–5]. Moreover, its low-temperature functionality is significantly limited by an incomplete urea decomposition at below 200 °C [4]. Because of these disadvantages of urea-SCR, many researchers have tried to utilize non-urea (NH_3) reductants such as engine-produced counterparts and/or fuel hydrocarbon itself [6–8].

A lean NOx trap (LNT) system is one of the commercially available deNOx technologies without an external reductant supply, capable of dealing with NOx emission in low-temperature ranges. However, this system requires complex engine control switching between lean/rich conditions to remove stored NOx/SOx periodically [9]. Using on-board hydrocarbon as a reductant (HC-SCR) may be an alternative strategy for removing NOx [6,10], but poor deNOx performance has been an obstacle to its practical implementation to the after-treatment system [11]. Another deNOx technology using H_2 reductant suffers from both poor N_2 selectivity and a narrow operating-temperature window,

* Corresponding author.
E-mail address: zaiseok@krict.re.kr (I. Heo).
[1] These authors contributed equally to this work.

https://doi.org/10.1016/j.apcatb.2020.119374
Received 25 May 2020; Received in revised form 21 July 2020; Accepted 24 July 2020
Available online 31 July 2020

although it would reduce NOx at low temperature [7].

Moving our attention to other available exhaust gas constituents, CO is the most abundant reductant, of which the engine-out concentration can be easily manipulated by controlling post-injection of fuel during combustion thanks to common-rail systems. The emission of CO further increases with the use of advanced combustion technologies such as HCCI (homogeneous charge compression ignition) for high energy efficiency with low NOx emissions [12,13]. NOx reduction by CO has long been well utilized in emission control systems using three-way catalysts (TWC). However, this works only when operating under a stoichiometric condition. In fact, CO is prone to be uselessly consumed in a fuel lean condition due to its high reactivity with O_2 compared to other reactants such as HC and NH_3. Thus, it is difficult to use CO for selective NOx reduction in after-treatment systems of diesel and lean-burn engines, where excess O_2 exists in the exhaust. This is why a number of previous studies dealt with the NOx-CO reaction under O_2-free conditions [14–16].

Despite less selectivity of CO toward NOx reduction in the presence of O_2, some studies have been conducted on a CO-derived deNOx process under a lean condition, which is called CO-SCR [17–20]. Haneda et al. explored a possible catalyst component for CO-SCR and found that Ir supported on SiO_2 was active in the presence of O_2 and SO_2 [17]. Wang et al. also reported the superiority of Ir as an active component for CO-SCR [18]. Further improved CO-SCR activity was reported with an Ir catalyst containing W and Ba, which became more active by adding H_2 into the feed stream [19,20]. However, although the Ir catalysts were relatively favorable for CO-SCR compared to other catalysts, its activity occurred in a narrow temperature range with poor NOx to N_2 conversion below 200 °C [7]. Thus, CO-SCR with Ir catalysts has not been proven as a promising candidate to replace urea-SCR, which shows almost complete conversion of NOx to N_2 at 200 °C [21].

However, a novel catalyst for lean NOx reduction by CO was recently developed [22], incorporating Ir and Ru on alumina to obtain a bimetallic catalyst configuration. The Ir-Ru/Al_2O_3 catalyst was very active for the NOx reduction by CO at low temperatures (< 200 °C) and showed almost comparable activity to urea-SCR under a lean condition, considering its application associated with advanced combustion technologies emitting relatively lower NOx and higher CO concentration than conventional analogues [12,13]. Moreover, this catalyst was thermally stable without any loss of Ir or Ru upon oxidative thermal aging simulating fleet vehicle mileage of 120,000 miles. In addition, Song et al. [23] recently showed that the deNOx activity over Ir-Ru/Al_2O_3 depends on its chemical composition. They reported that an Ir-Ru alloy was formed on that catalyst, which possesses an extraordinary catalytic property, as compared to the case with dual sites consisting of independent Ir and Ru metal particles. The high reactivity of this catalyst system has newly brought attention to NOx reduction by CO for automotive lean NOx application. However, it is still unclear how the Ir-Ru bimetallic catalyst derives distinct low-temperature functionality via NOx reduction by CO, especially under the lean condition.

In the present study, Ir-Ru/Al_2O_3 catalysts were tested and characterized to elucidate the origin of their high activity in lean NOx reduction by CO. We systematically compared physicochemical properties of an Ir-Ru bimetallic catalyst to those of monometallic counterparts containing either Ir or Ru, along with their surface adsorption-reaction features. We tried to rationalize the synergism between Ir and Ru stemming from the alloy structure, on the basis of careful investigation of multiple elementary reaction steps over each catalyst for lean NOx reduction by CO including NO dissociation and surface-covering oxygen removal. Finally, our experimental results have further been verified by computational calculations using density functional theory (DFT).

2. Experimental

2.1. Catalyst preparation

Noble metal supported catalysts were prepared by the incipient wetness impregnation method using gamma alumina (STREM, 97.7 %, BET surface area = 200 m^2/g) as a support. Alumina support was selected due to its high stability (thermal and chemical) proven in a variety of applications along with its relatively lower price, both of which are essential prerequisites for the real field application. Active metal precursors were iridium (III) chloride hydrate (Alfa Aesar, 99.9 % metals basis) and ruthenium (III) chloride hydrate (Alfa Aesar, 99.9 % metals basis). In brief, metal precursors were dissolved in distilled H_2O, the amount of which was calculated based on the pore volume of the support. The metal precursor solution was then mixed with Al_2O_3 to make an aqueous slurry. As-made catalysts were dried at 110 °C overnight, and subsequently calcined at 500 °C for 5 h. In particular, the Ir-Ru bimetallic catalyst was prepared by the co-impregnation method with a 1:1 molar ratio of Ir and Ru. Note that all three catalysts contain the equivalent number of total metal atoms, regardless of the metal type. The total metal content was set to 3.05 wt.% for Ir-Ru/Al_2O_3, given deNOx activities between 150 and 200 °C depending on metal loadings (Fig. S1). Details of the metal contents in the prepared catalysts are described in Table 1. It is also noteworthy that the pore properties of the calcined catalysts are similar to the bare alumina (Table 1), indicating that pore blocking/plugging during the PGM impregnation is trivial.

2.2. Activity measurements

The NOx reduction activity of each catalyst by CO was evaluated in a packed bed powder reactor system under steady state conditions maintaining the reaction temperatures at each set point for 30 min. Catalyst powder (0.225 mL) was charged in a SUS tube reactor with a total gas flow rate of 750 mL/min, corresponding to gas hourly space velocity (GHSV) of 100,000 h^{-1}. Prior to the activity test, the catalyst was reduced at 450 °C for 1 h in 10 % H_2/N_2 for its activation as previously reported [23,24]. The standard reaction feed stream for lean NOx reduction by CO consisted of 50 ppm NO, 0.7 % CO, 5% O_2, 10 % H_2O, and N_2 balance, simulating the automotive exhaust for advanced combustion engines, i.e. relatively low NOx concentration with an abundant amount of CO [13,23]. The compositions of the feed were sometimes changed depending on a type of reaction. Inlet and outlet gas concentrations were monitored by FT-IR (Nicolet iS 10, Thermo Fisher Scientific) equipped with a deuterated triglycerine sulfate (DTGS) detector and a gas cell of 2 m path length (Thermo Fisher Scientific). NOx (NO + NO_2), CO conversions and NO_2 and N_2 selectivity of the reaction were calculated by the following equations:

Table 1
The properties of the catalysts employed in this study.

Catalyst	Theoretical PGM content (wt.%)	BET surface area (m^2/g)	Total pore volume (cm^3/g)	CO chemisorption ($\mu mol/g_{cat}$)	Dispersion (%)
Al_2O_3	–	210	0.48	–	–
Ir/Al_2O_3	4.00	197	0.47	11.0	5.3
Ru/Al_2O_3	2.10	198	0.44	7.7	3.7
Ir-Ru/Al_2O_3	2.00 (Ir), 1.05 (Ru)	196	0.44	13.8	6.7

$$\text{NOx/CO Conversion (\%)} = \frac{[X]_{in} - [X]_{out}}{[X]_{in}} \times 100 \quad \text{(A.1)}$$

$$\text{NO}_2\text{ selectivity (\%)} = \frac{[NO2]_{out}}{[NO]_{in} - [NO]_{out}} \times 100 \quad \text{(A.2)}$$

$$\text{N}_2\text{ selectivity (\%)} = \left(1 - \frac{[NO2]_{out} + 2 \times [N2O]_{out} + [NH3]_{out}}{[NO]_{in} - [NO]_{out}}\right) \times 100 \quad \text{(A.3)}$$

* [X]: concentration of NOx or CO

2.3. Catalyst characterization

The pore properties of the catalysts was determined from the N_2 isotherm, measured by a volumetric adsorption apparatus at 77 K (3Flex, Micromeritics). The specific surface area was calculated by the Brunauer-Emmet-Teller (BET) equation, and the total pore volume was determined at $P/P_0 = 0.99$. Before measurements, all samples were degassed for more than 12 h at 623 K under a vacuum condition. A CO-chemisorption analysis was carried out to relatively compare the metal dispersion. After the catalysts were pretreated at 450 °C for 1 h in a 10 % H_2/Ar flow, the temperature was cooled to 50 °C with He, and then a fixed amount of 5% CO/He gas was injected periodically into the catalysts until the adsorption saturation.

The crystal structure of each catalyst was determined by the X-ray diffraction (XRD) and the extended X-ray absorption fine structure (EXAFS) analysis. X-ray diffraction data were collected using a Rigaku Rotaflex with a wavelength of 1.54059 Å (Cu). The powder sample was placed evenly on a quartz holder. Scans ranged from 20° to 80° with a 0.02° step size and a 1°/min step rate. The EXAFS spectra of the Ir L3-edge were obtained at room temperature in fluorescence mode at 7D XAFS beamline of Pohang Light Source (PLS). The obtained EXAFS data were normalized and fitted by using Athena and Artemis software. The theoretical path of Ir–Ir was calculated from the structure of bulk Ir metal (fcc structure). The Ir–Ru path was calculated by replacing Ir with Ru in the Ir fcc structure.

In situ diffuse reflectance infrared transform spectroscopy (DRIFTs) experiments were conducted to identify surface adsorbed species on the catalysts using a Nicolet 6700 spectrometer equipped with a mercury cadmium telluride (MCT) detector cooled by liquid N_2 and a commercial DRIFT cell (PIKE, DiffuseIR). DRIFT data were collected in the Kubelka − Munk format with 32 scans averaged per spectrum at 4 cm^{-1}. Prior to each experiment, the catalyst was pretreated under the same conditions to the activity measurements. It was then exposed to reactants such as CO, NO, and O_2.

Temperature-programmed experiments were conducted on an AutoChemII 2920 (Micromeritics). For the temperature-programmed desorption (TPD) analysis, each catalyst was first pretreated at 450 °C for 1 h in 10 % H_2/Ar to obtain a reduced form, and subsequently purged with He while being cooled to 175 °C. The reduced catalyst was then exposed to 30 mL/min of 500 ppm NO/He feed mixture for 1 h at the same temperature. Once this feed was injected, the real-time signals of gas species started to be detected by a mass spectrometer (HPR-40, HIDEN). After the NO adsorption, the catalyst was purged with He to remove the physiosorbed species. Finally, the temperature was increased up to 900 °C with a 5 °C/min ramping rate. To investigate the reactivity of CO with surface-covering oxygen dissociated from NO, similar steps to NO-TPD experiments were performed. 50 ppm NO/N_2 feed was flowed to the reduced catalyst for 1 h at 175 °C, followed by purging with N_2. The temperature was then raised to 400 °C under a N_2 flow for desorbing all NO molecules while keeping surface-covering oxygen from NO dissociation, based on the previous NO-TPD results. After the catalyst was cooled to 50 °C with N_2, the feed was changed to 0.7 % CO/N_2, and then the temperature was increased up to 400 °C once all gas concentrations were stabilized. In the meantime, the concentration of CO_2 generated mostly by the reaction between CO and chemisorbed oxygen was measured by a FT-IR spectrometer (Nicolet iS 10, Thermo Fisher Scientific).

2.4. Computational details

Periodic density functional theory (DFT) calculations were carried out using the vdW-DF2 functional [25] as implemented in the Vienna Ab-initio Simulation Package (VASP) [26]. The valence density was expanded in a plane wave basis set with a kinetic energy cutoff of 450 eV. The convergence criterion was set to 10^{-4} eV and the effect of the core electrons in the valence density was taken into account by means of the projected augmented wave formalism. The Ir (111), Ru (001) and 25 % Ru-doped Ir (Ir_3Ru_1) surfaces were simulated by creating a 4 × 4 × 4 supercell slab model, which was separated by a vacuum region of 10 Å to avoid interaction between periodically repeated slabs. Prior to building the surface structure, bulk Ir (Fm-3 m), Ru (P63/mmc), and L12 structured Ir3Ru1 alloy (Fm-3 m) were optimized and resulted in lattice parameters close to the experimental values (Ir, a = b = c = 3.987; Ru, a = b = 2.786, c = 4.397). For the bulk and surface slab calculations, the Brillouin zone samplings were carried out using a Monkhorst-Pack k-points mesh grid of 16 × 16 × 16 and 4 × 4 × 1, respectively. During the geometry optimizations, the positions of the adsorbates and of the Ir, Ru, and Ir_3Ru_1 atoms of the two uppermost layers were allowed to fully relax. The free energy of reaction, ΔG, was calculated using the following equation

$$\Delta G = \Delta E + \Delta ZPE + \Delta \int C_p dT - T\Delta S \quad \text{(B.1)}$$

where, ΔE, ZPE, C_p, T, and S denote the *an-initio* energy difference between the initial and final states, the zero-point energy, the heat capacity, temperature, and entropy, respectively. Transition states for N−O bond scission, O−CO bond formation, N−N bond formation, and N−NO recombination on catalyst surfaces were calculated using the climbing-images nudged elastic band (CI-NEB) method. Confirmation of the transition state structure was carried out by a vibrational frequency analysis where transition states show single imaginary frequency. Free energies of gas and adsorbed species were calculated under the ideal gas limit and harmonic limit, respectively, assuming reaction conditions of 175 °C and 0.1 MPa.

3. Results and discussion

3.1. Catalyst activities for lean NOx reduction by CO

Presented in Fig. 1 is the NOx reduction activity of the three catalysts, Ir/, Ru/, and Ir-Ru/Al_2O_3, under the standard feed stream simulating the exhaust gas of advanced combustion engines. The Ir-Ru bimetal catalyst supported on Al_2O_3 reveals superior NOx reduction performance over both Ir and Ru monometallic counterparts in the entire reaction temperature, despite that the molar content of PGM was the same in all catalysts. In particular, the Ir-Ru/Al_2O_3 catalyst achieves 91 % NOx conversion at 175 °C, while no activity is observed over the monometallic analogues. NOx conversion over Ir-Ru/Al_2O_3 decreases with the increase of reaction temperature from 175 °C attributed to the formation of byproduct NO_2, as depicted in Fig. 1(d). Although the NO_2 selectivity of Ir-Ru/Al_2O_3 has become nearly 40 % at 300 °C, it is still lower compared to the case with the other two catalysts. The N_2O concentration over Ir-Ru/Al_2O_3 is also described in Fig. 1(d). N_2O is produced below 5 ppm over the entire reaction temperature, resulting in high N_2 selectivity of Ir-Ru/Al_2O_3 below 250 °C. Indeed, the N_2 selectivity of Ir-Ru/Al_2O_3 is calculated as 78 and 89 % at 175 and 200 °C, respectively (NH_3 was not observed in all conditions). Moreover, the effect of other exhaust gas components (H_2, C_3H_6) on the deNOx activity of Ir-Ru/Al_2O_3 appeared to be negligible at 200 °C (Fig. S2). Given the long-term durability of the Ir-Ru catalyst under the lean condition reported elsewhere [24], a high probability would be expected that this

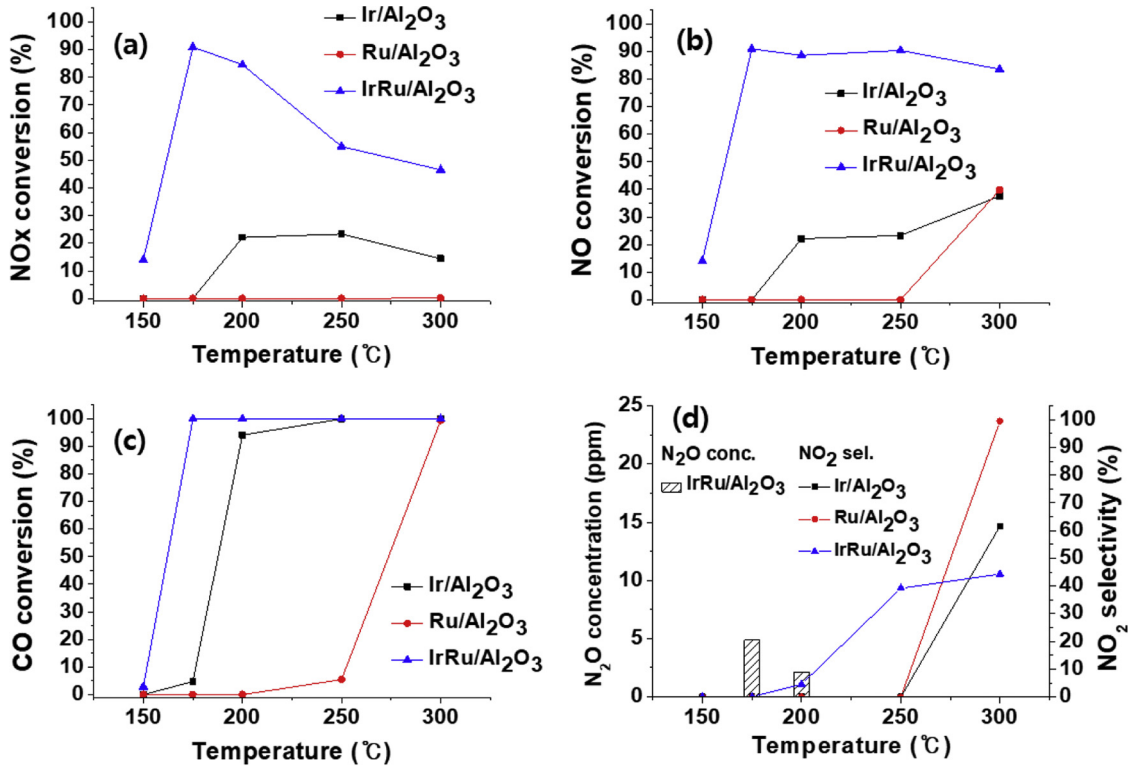

Fig. 1. (a) NOx, (b) NO, and (c) CO conversion, and (d) N_2O concentration and NO_2 selectivity over Ir/, Ru/ and Ir-Ru/Al_2O_3 catalysts. Feed composition: 50 ppm NO, 0.7 % CO, 5% O_2, 10 % H_2O, and N_2 balance. GHSV = 100,000 h^{-1}. Catalyst pretreatment: 450 ℃ for 1 h in 10 % H_2/N_2.

catalyst would work well in the after-treatment system once CO can be sufficiently utilized. In the case of the CO reactivity, the bimetallic catalyst shows distinct behavior (Fig. 1(c)). Ir-Ru/Al_2O_3 is capable of almost 100 % CO conversion at 175 ℃, whereas the Ir or Ru monometallic catalyst shows a value only below 10 %. More interestingly, both CO oxidation and NOx reduction reactions start to be activated over Ir-Ru/Al_2O_3 at a similar temperature, comparing Fig. 1(a) with (c). These unique features of Ir-Ru/Al_2O_3, i.e., a high CO oxidation rate and similar light-off temperature for CO and NOx, are likely to be associated with its high NOx reduction performance, as will be discussed later.

From the results of the activity test, the synergistic effect of Ir and Ru on low-temperature lean NOx reduction by CO has been confirmed, consistent with the previous results [22,23]. Indeed, the Ir-Ru/Al_2O_3 catalyst showed a much higher TOF and lower apparent activation energy for the NO conversion under the NO−CO−O_2 reaction conditions, compared to the monometallic catalysts (Fig. S3). This implies that the reaction kinetics of the Ir-Ru bimetallic site may be quite differ from the monometallic counterparts under the lean deNOx condition. According to a previous study [23], both NOx and CO conversions over the physical mixture of Ir/Al_2O_3 and Ru/Al_2O_3 could never meet those over Ir-Ru/Al_2O_3, indicating that the synergism between Ir and Ru may originate from their interaction within the molecular level.

To better understand the details of lean NOx reduction by CO reaction over the Ir-Ru catalyst, simple-feed tests have also been conducted (NO−CO and CO−O_2 reactions), as depicted in Fig. 2. In the NO−CO reaction, Ru/Al_2O_3 shows 36 % NO conversion at 175 ℃, comparable to Ir-Ru/Al_2O_3. However, as can be seen in Fig. 1, no activity was exhibited over Ru/Al_2O_3 under an O_2-containing feed condition (standard feed). This indicates that the feature of surface Ru has been significantly changed upon the addition of O_2 in the feed stream. Indeed, a Ru supported catalyst is reported to have higher O_2 affinity on its catalytic surface than other platinum group metals counterparts [27]. This surface-covering oxygen can diminish the deNOx ability of Ru/Al_2O_3, as will be discussed later. As shown in Fig. 2(b), the CO conversion of Ru/Al_2O_3 is higher under a CO-O_2 condition than a standard feed condition containing NO. This might be due to the competitive adsorption of NO and CO, since strongly adsorbed NO on the Ru site could interfere with the adsorption of CO [28]. In addition, increased oxygen coverage on the Ru surface originated from the dissociation of NO might be another reason. Indeed, the NO decomposition reaction is reported to occur over the Ru-based catalyst [29,30]. The abundance of oxygen on Ru can hinder the CO oxidation reaction [31]. Even under a reducing or mild oxidizing condition, an increase of O_2 concentration is not highly beneficial for the CO oxidation over Ru, compared to other platinum group metals following the first order kinetics on O_2 [32].

On the other hand, NOx conversion of Ir-Ru/Al_2O_3 is higher under the standard feed condition (NOx conv. = 91 %) than that under the NO−CO condition (NOx conv. = 38 %), which is opposite to Ru/Al_2O_3. This means that not only does Ir-Ru/Al_2O_3 have superior O_2 tolerance, but also O_2 has a positive impact on NOx reduction over Ir-Ru/Al_2O_3. Moreover, Ir-Ru/Al_2O_3 shows outstanding activity of CO oxidation (Fig. 2(b)). Almost 100 % CO conversion is achieved even at the reaction temperature of 125 ℃. As previously mentioned, since the NOx reduction occurs simultaneously with the CO conversion under the standard feed condition (Fig. 1), the high activity of CO oxidation can be one of the reasons why lean NOx reduction by CO favorably occurs over Ir-Ru/Al_2O_3 in the low temperature region.

Unlike the other catalysts, Ir/Al_2O_3 has similar light-off temperature for NO under both standard and simple-feed (NO−CO) conditions. This means that poisoning effect of O_2 seen in the Ru monometallic catalysts is not noticeable in the Ir monometallic catalyst, although the reductant CO has been aggressively consumed by the oxidation reaction. This feature is likely why Ir catalyst has been extensively studied as the CO-SCR catalysts. However, Ir/Al_2O_3 exhibits the lowest NO−CO reactivity, from which it can be inferred that NO activation on the Ir site is more difficult than with other catalysts. Also of interest is that the CO oxidation activity under a simple-feed condition over Ir/Al_2O_3 is quite similar to the case with the full-feed counterpart (Figs. 1(c) and 2 (b)). Two possible explanation can be made for this catalytic behavior as

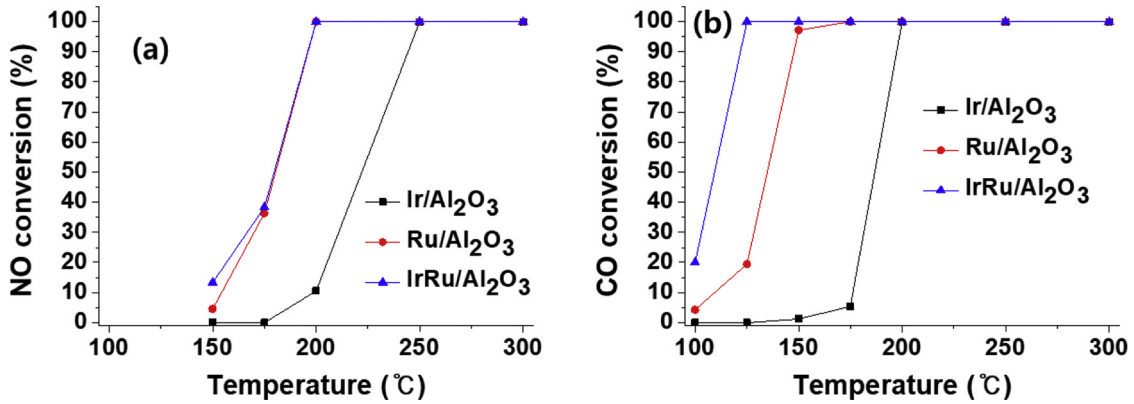

Fig. 2. NO and CO conversion over Ir/, Ru/, and Ir-Ru/Al_2O_3 catalysts. Feed composition: (a) 50 ppm NO, 0.7 % CO, and N_2 balance. (b) 0.7 % CO, 5% O_2, and N_2 balance. GHSV = 100,000 h^{-1}. Catalyst pretreatment: 450 ℃ for 1 h in 10 % H_2/N_2.

follows: (1) The competitive adsorption of CO over NO is trivial on the Ir surface, and/or (2) The dissociation of NO into oxygen and nitrogen does not occur effectively on the Ir surface, the latter of which is unsuitable for the NO reduction by CO [33,34]. In order to understand the catalytic behaviors of those three samples, they were analyzed by various characterization tools, as will be shown in the next sections.

3.2. Structural and physicochemical properties of Ir-Ru catalysts

XRD patterns of the catalysts were obtained to gain information on crystal structures. Shown in Fig. 3(a) are the diffraction patterns of the catalysts reduced at 450 ℃. Ir/Al_2O_3 has a *fcc* (face-centered cubic)-structured metallic Ir phase, as evidenced by diffraction peaks at 40.6 and 47.1° corresponding to the Ir (111) and Ir (200) plane, respectively [35,36]. The Ru monometallic catalyst shows a diffraction peak at 44.1°, assigned to Ru (101) in an *hcp* (hexagonal close-packed) structure [35,36]. Ir and Ru diffraction peaks are observed individually in the Ir-Ru bimetallic catalyst pre-reduced at 450 ℃, and these peaks become clearer when being reduced at 850 ℃ due to the growth of the crystallite size. However, the Ir diffraction peak of Ir-Ru/Al_2O_3 is shifted to a slightly higher angle than that of Ir/Al_2O_3 (40.6°), indicating that the lattice parameter of the Ir phase of Ir-Ru/Al_2O_3 is shrunk slightly [37,38]. The change of the lattice parameter is likely due to the formation of a *fcc*-structured Ir-Ru alloy [36,38]. Although the molar concentrations of both Ir and Ru are identical in Ir-Ru/Al_2O_3, the Ir-Ru alloy does not seem to be homogenous, since the XRD patterns of equimolar Ir-Ru alloy should appear at a 2 theta between Ir and Ru diffraction peaks according to Vegard's rule. Thus the crystallite structure corresponding to the diffraction peak of Ir-Ru/Al_2O_3 at around 41° can be attributed to the Ir-Ru alloy enriched by Ir. The shift of the Ir diffraction peak to a higher angle is caused by the reduction of the lattice parameter due to the partial substitution of the Ir atom with the smaller Ru analogue [37,38]. Upon the addition of Ir, similarly, the diffraction of Ru (101) spreads to a slightly lower angle, indicative of a Ru-enriched alloy in a hcp arrangement, due to the fractional replacement of Ru atoms by the Ir counterpart. Therefore, both Ir-rich and Ru-rich metallic Ir-Ru alloys appear to exist in the Ir-Ru/Al_2O_3 catalyst. Although the quantitative contribution of the two alloy phases on the deNOx activity was not fully determined in this study, both Ir rich and Ru rich phases are considered to be responsible for the high deNOx activity compared to Ir only and Ru only phases [23]. A TEM-EDS analysis was carried out to investigate the distribution of Ir and Ru in the Ir-Ru/Al_2O_3 catalyst (Fig. S4). Although these two metals are not evenly distributed, the overlap of Ir and Ru may have been brought by the metal alloy thereof.

For a further examination of the structure of Ir-Ru/Al_2O_3, EXAFS analysis of Ir L_3-edge was conducted, and the profiles of Fourier transform (FT) of k^3 weighted EXAFS oscillations are represented in Fig. 3(b). Ir/Al_2O_3 shows the FT profile, which closely matches the bulk sample of Ir metal in terms of both the intensity and position of the peaks, in particular between 2 and 3 Å, corresponding to the first neighboring atom of Ir. In addition, Ir/Al_2O_3 does not have a significant peak at 1.6 Å attributed to the first neighboring atom of O, in contrast to the IrO_2 reference. These mean that the crystal structure of Ir metal in Ir/Al_2O_3 is similar to the bulk metallic Ir. On the other hand, the overall trend of the FT profile of Ir-Ru/Al_2O_3 is analogous to that of the standard Ir metal sample, but the peak positions are shifted and the intensity is significantly lowered compared to the Ir metal, demonstrating that the local environment around the Ir atom has been changed. These differences in the FT profile are likely due to the formation of Ir-Ru

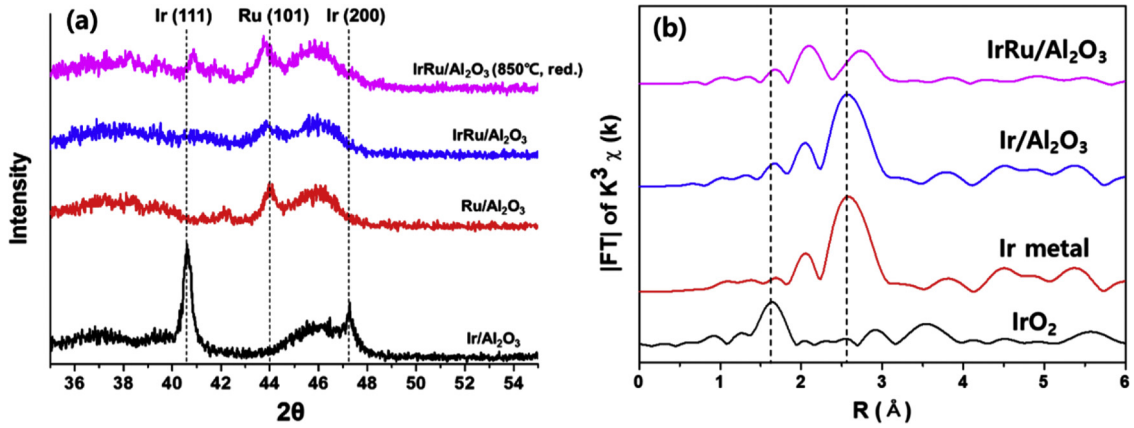

Fig. 3. (a) XRD patterns and (b) EXAFS Fourier transform of ex-situ reduced Ir/, Ru/, and Ir-Ru/Al_2O_3.

Table 2
EXAFS fitting results of Ir L_3-edge of reduced Ir/ and Ir-Ru/Al_2O_3.

Catalyst	Shell	CN	R (Å)	R-factor (%)
Ir/Al_2O_3	Ir-Ir	11.0 ± 1.5	2.70 ± 0.01	1.12
Ir-Ru/Al_2O_3	Ir-Ir	7.7 ± 1.9	2.69 ± 0.02	1.68
	Ir-Ru	2.5 ± 2.0	2.68 ± 0.02	

alloy [36,39]. To analyze the local structure of Ir in detail, EXAFS curve fitting has been carried out. The measured and fitted data are plotted together in Fig. S5, and the fitting results are summarized in Table 2. EXAFS of Ir/Al_2O_3 was fitted well (R-factor = 1.12 %) with only the Ir-Ir path. The coordination number (CN) of Ir-Ir was estimated as 11, reflecting a bulk Ir metal structure in Ir/Al_2O_3, as described above. However, both Ir-Ir and Ir-Ru paths should be taken into account to satisfy the EXAFS fitting of Ir-Ru/Al_2O_3, indicating the existence of Ir–Ru bonding in Ir-Ru/Al_2O_3. The CN expected from the Ir-Ru bulk ratio (1:1 mol ratio) is quite different from the fitting results. The CN of Ir-Ir path is 7.7, which is much higher than that of the Ir-Ru path (CN = 2.5). Therefore, an Ir-enriched Ir-Ru alloy can be deduced as the local structure of Ir, which is in line with the XRD results.

The crystallite structure of each catalyst without H_2 pretreatment was also analyzed by XRD as shown in Fig. 4(a). Ir/Al_2O_3 calcined at 500 °C in air flow shows IrO_2 phase, while RuO_2 phase is detected on Ru/Al_2O_3 [19,40]. The peaks of Ir-Ru/Al_2O_3 (calcined in air flow) appear almost at the center between IrO_2 (101) and RuO_2 (101) peaks, indicating the formation of homogeneous solid-solution even in the oxide form. This solid-solution mixed oxide structure has been also confirmed by the TPR result (Fig. 4(b)). The reduction feature of Ir-Ru/Al_2O_3 (calcined in air flow) by H_2 appears as nearly single peak, the position of which is between the cases with of Ir/Al_2O_3 and Ru/Al_2O_3. This is probably due to the reduction of Ir-Ru solid-solution mixed oxide phase, in line with XRD. Although the oxide form of PGM metals have been known to be inactive for NOx reduction by CO [7,19], the formation of an active Ir-Ru metal alloy originates from this mixed oxide. The H_2 pretreatment may then induce the reconstruction of metal oxides followed by the alloy formation [41].

Ir alloyed with Ru is reported to be thermodynamically feasible compared to that with other platinum group metals such as Pt, Pd, and Rh [42]. When the bimetallic alloy is formed, both the adsorption property and surface chemistry of reactants are prone to be changed significantly compared to the case with the monometallic phase, mainly attributed to two aspects, strain and ligand effects. The lattice parameter and bonding length of the monometallic phase can be changed upon the strain induced by its partial substitution with other metals, leading to the alteration of their electronic orbitals [42]. In addition, the intrinsic electronic property of each metal can be changed by the presence of another nearby metal, possible due to their interaction with each other, which is called the ligand effect [42]. On the other hand, the pretreatment with H_2 is reported to induce the surface enrichment and ordering of Ir atoms in Ir-Ru alloy [43]. In that case, the ligand effect might play a predominant role in changing the surface chemistry on the Ir-Ru alloy, since the top layer of Ir atoms are only under strain in the vertical direction, leading to a surface lattice parameter that is unchanged from the monometallic case [42]. Further study including computational calculations is required to clearly elucidate these effects related to the Ir-Ru alloy. Nonetheless, these electronic effects are likely to induce alterations of the adsorption property and surface chemistry of reactants on each catalyst, as will be discussed in the following sections.

3.3. Surface adsorbed species of the catalysts

The adsorbed species on the surface of the catalysts was investigated under the NO−CO−O_2 reaction condition using in situ DRIFTs. Note that H_2O was excluded in the reaction feeds to prevent peak noises by moisture in the IR cell. Notably, H_2O has a trivial impact on the NOx reduction activity in the Ir-Ru catalyst system, as shown Fig. S2. Before the measurement, each catalyst was reduced under the same conditions as in the activity test and cooled under a N_2 flow to 150 °C. After stabilization of the DRIFTs cell temperature, a gas mixture composed of NO−CO−O_2 was fed for 1 h, followed by purging with N_2 for 1 h. Fig. 5(a) shows the DRIFT spectra of each sample exposed to the NO−CO−O_2 feed. The peaks corresponding to gaseous CO are observed in $2220-2050\,cm^{-1}$, of which the low wavenumber range is overlapped with IR bands attributed to CO adsorbed onto catalysts. The adsorbed species can further be clearly identified after each sample has been purged with N_2, as described in Fig. 5(b). The peaks due to linear-CO on the metallic sites ($Ir^0$and Ru^0) were observed at 2004–2086 [17,44,45]. The several peaks related to C−O vibration on each catalyst may be indicative of either multiple adsorption sites (linear and bridge types) [46,47] or the presence of co-adsorbed species such as OH, O, Cl, and NO [17,48,49]. The peaks between 1873 and $1795\,cm^{-1}$ can be interpreted as linear-bonded NO on atop sites, which have higher vibrational frequency than that associated with bridge and hollow counterparts [50,51]. In addition, the broad band with multiple peak shoulders are observed in the region below $1600\,cm^{-1}$. It can be guessed that these peaks are related to carbonate- and nitrate-type species associated with both alumina and metallic sites, although they are difficult to discriminate due to their peak position overlapping with each other [52–54].

Between Ir/Al_2O_3 and Ru/Al_2O_3, a significant difference is observed in terms of the NO peak position, whereas the Ir-Ru bimetallic catalyst reveals both features. In detail, Ru/Al_2O_3 shows NO adsorption peaks at

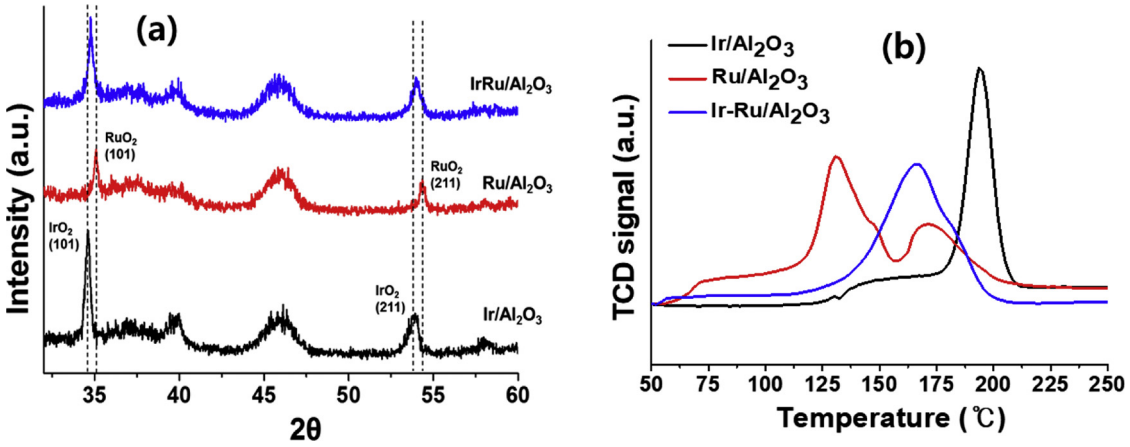

Fig. 4. (a) XRD patterns and (b) H_2-TPR of oxidized Ir/, Ru/, and Ir-Ru/Al_2O_3.

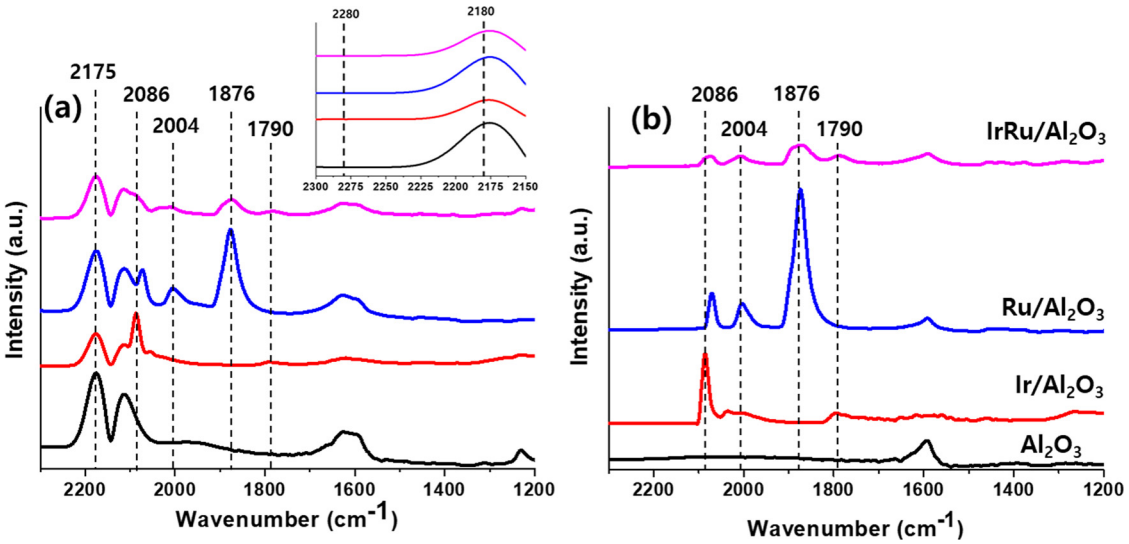

Fig. 5. FT-IR spectra of the catalysts and alumina (a) after exposure of the NO – CO-O_2 feed stream (50 ppm NO, 0.7 % CO, 5% O_2 and N_2 balance) and (b) followed by N_2 purging at 150 °C for 1 h.

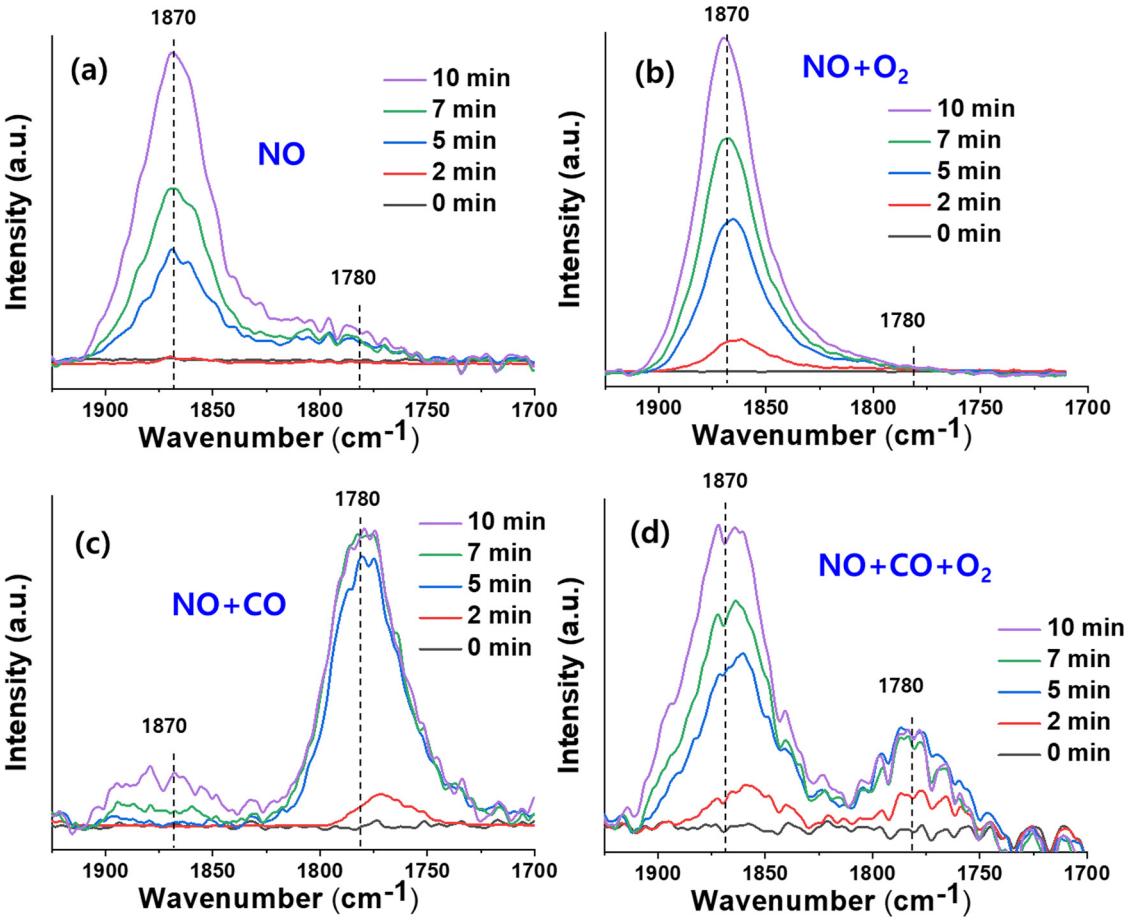

Fig. 6. DRIFT spectra of NO adsorbed onto the Ir-Ru catalyst after exposure of various feed compositions at 175 °C: (a) NO, (b) NO + O_2, (c) NO + CO, and (d) NO + CO + O_2 (50 ppm NO, 0.7 % CO, 5% O_2 and N_2 balance).

much higher wavenumber (1873 cm^{-1}) compared to the case with Ir/Al_2O_3 (1795 cm^{-1}). This is well matched to the peak position reported for NO on the oxygen-covered Ru metal, whereas it would appear at a lower wavenumber around 1800 cm^{-1} in the case of an oxygen-free surface [44,55]. Similarly, the vibrational frequency due to NO adsorbed on Ir metal may be higher than that observed over Ir/Al_2O_3 in this study, when the surface is oxidized [56]. This peak shift of NO induced by the surface oxygen is clearly observed in the IR spectra of Ir-Ru/Al_2O_3 exposed to various feed compositions (Fig. 6). The peak at 1870 cm^{-1} is dominantly observed in the NO flow (Fig. 6(a)), which might be due to the oxygen-covered surface via the dissociation of NO. The intensity of this peak has become more pronounced when O_2 flow

is added possibly due to the dissociative adsorption of O_2 (Fig. 6(b)). With the NO + CO feed condition (Fig. 6(c)), in contrast, another peak at much lower wavenumber (1780 cm^{-1}) is prominently exhibited, indicating that the metallic phase was well maintained possibly due to the removal of surface oxygen by CO. In the case of NO + CO + O_2 flow (Fig. 6(d)), the reaction condition of lean deNOx by CO, both peaks of 1780 and 1870 cm^{-1} are exhibited obviously. In other words, oxygen-covered and oxygen-free surfaces coexist over Ir-Ru/Al_2O_3 under this reaction condition. Indeed, the electron-withdrawing oxygen can reduce the electron density of nearby metals, which facilitates the donation of electrons from NO antibonding molecular orbital to their local d-band. This results in the strengthening of the N—O bond, and thereby the blue-shift of the NO stretching vibrational frequency [55,57]. Given this, it might be anticipated that Ru/Al_2O_3 is covered by oxygen more readily than Ir/Al_2O_3 under the feed condition (NO − CO-O_2), which is highly unfavorable for the NOx reduction by CO. Another possible explanation of the difference in the NO adsorption band between both catalysts would be the effect of molecules neighboring NO [17,58].

On the other hand, the DRIFTs results can give hints suggesting the reaction pathway of lean NOx reduction by CO over Ir-Ru/Al_2O_3. Indeed, the CO—NO adsorption properties of our catalysts do not appear to correlate well with their deNOx activity. Although both NO and CO appeared to be simultaneously adsorbed well on the surface of the Ru catalyst, there was no deNOx activity (Fig. 1(a)). This might imply that the direct reaction between NO and CO with the Langmuir-Hinshelwood mechanism is unlikely to be predominant over the catalysts. A similar conclusion, a low possibility of direct NO—CO reaction, has been reported for Pd and Rh catalysts in the literature [34,59]. Excluding the direct NO—CO reaction pathway, another route involving a NCO intermediate and its subsequent reaction with NO [NCO* + NO* → N_2 (g) + CO_2 (g)] can be proposed as the reaction pathway of NOx reduction by CO [17,33,54]. However, none of the catalysts showed an IR band at around 2240 cm^{-1} that is supposed to appear when NCO species exist [60,61], as depicted in Fig. 5(a). Some research groups suggested that these NCO species on metals reveal IR vibrational frequency at around 2180 − 2200 cm^{-1} [17,45]. In this case, it cannot be directly detected in our DRIFT study, mainly due to the peak overlap with CO gases (2220 − 2050 cm^{-1}). However, these NCO species are known to move readily from metals to supports [46,62–65]. As shown in Fig. 5, the IR band corresponding to Al-NCO was not observed as well (2240 − 2280 cm^{-1}), which should be stable as a spectator [46,66–68]. Similar results have been obtained even after changing the reaction temperature to 175 °C (Fig. S6), where the highest deNOx performance was observed. Thus, we might be able to rule out the NCO-related reaction mechanism for lean NOx reduction by CO over Ir-Ru/Al_2O_3.

A"NO dissociative model" initiated from NO decomposition might then be a reasonable pathway of lean NOx reduction by CO over Ir-Ru/Al_2O_3. Indeed the dissociation of NO over Ir-Ru/Al_2O_3 could be suggested from the DRIFTs experiment with NO flow (Fig. 6(a)). As mentioned earlier, the predominant presence of the peak at around 1870 cm^{-1} may demonstrate that NO can be dissociated into N and O atoms readily, of which the latter continues to accumulate on the surface leading to the blue shift of NO adsorption peak. Recently, a similar suggestion was reported by Kondoh et al. [33], who claimed that the N* + N* reaction is the dominant pathway to N_2 formation during the course of NO reduction by CO over the Ir (111) surface. This reaction mechanism does not require any reaction intermediate induced by CO, such as NCO.

3.4. NO adsorption and dissociation thereof

When the NO reduction directly proceeds without reaction intermediates induced by CO such as NCO, the following reaction steps may be mainly involved [46,69]:

$$NO\ (g) \rightarrow N^* + O^*\ [\text{Dissociation of NO}] \quad (C.1)$$

$$N^* + N^* \rightarrow N_2\ (g)[\text{Recombination of surface N}] \quad (C.2)$$

$$O^* + CO^* \rightarrow CO_2\ (g)\ [\text{Reduction of surface O}] \quad (C.3)$$

The reduction of NO into N_2 can also occur via NO disproportionation [50,69] instead of reaction (C.2).

$$N^* + NO^* \rightarrow N_2\ (g) + O^*[\text{NO disproportionation}] \quad (C.4)$$

He et al. reported that that the reaction (C.2) is more favorable for NO reduction than the reaction (C.4), based on the DFT calculations and microkinetic analysis over Ir(100). However, Nakamura and Fujitani claimed that the NO disproportionation (C.4) occurs over Ir (111) at lower temperature compared to the recombination of surface N (C.2) [69]. In either case, the reduction of NO should be initiated with its dissociation into N and O atoms on the catalytic surface, which has been recognized as one of the rate-determining steps for the NO reduction by CO [33,34].

The adsorption of NO and dissociation thereof on the catalysts were investigated through NO-TPD experiments, as described in Fig. 7. The adsorption step of NO-TPD was conducted under a 500 ppm NO/He flow at 175 °C, followed by He purge at identical temperature, and then the desorption step ramping up the temperature up to 900 °C, while real-time signals of outlet gases were recorded by mass spectroscopy (Fig. 7). The amount of NO desorbed over Ir/Al_2O_3 throughout purging and desorption periods is equivalent to 96 % of that consumed during the adsorption step, as listed in Table 3. That is, NO dissociation rarely occurred on the Ir monometallic site. In contrast, Ir-Ru bimetallic and Ru monometallic catalysts exhibit a much lower NO_{de}/NO_{con} ratio (about 60 %) than Ir/Al_2O_3. This implies that NO can be dissociated more readily on Ir-Ru and Ru sites, which is more highly favorable for the NO—CO reactivity than Ir/Al_2O_3, as shown in Fig. 2(a). According

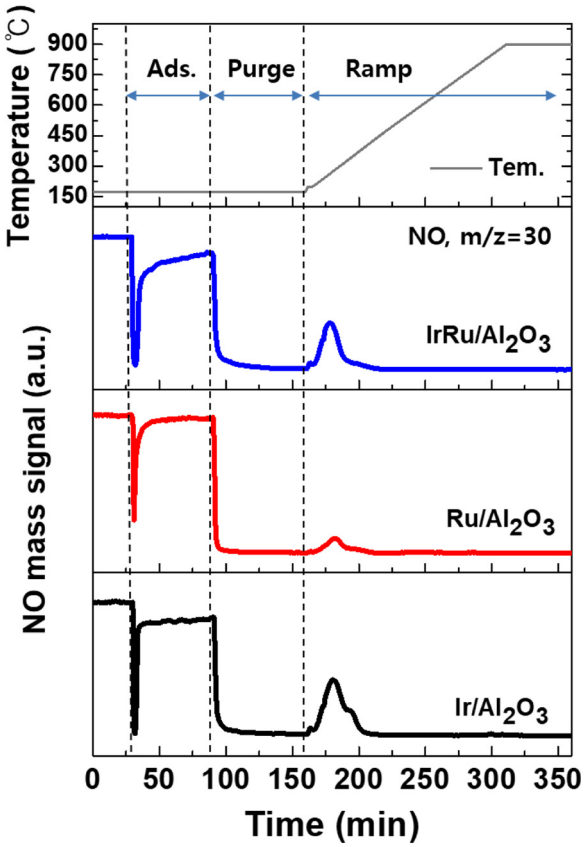

Fig. 7. The MS signal of NO (m/z = 30) during the NO-TPD experiments of the catalysts. Adsorption step: 500 ppm NO/He, 175 °C. Purging step: He, 175 °C. Ramping step: He, 175-900 °C, 5 °C/min, 1 h.

Table 3
The quantification of consumed and desorbed NO during the NO-TPD analysis.

Catalyst	NO consumption (μmol/g_{cat})	NO desorption (μmol/g_{cat})	NO des. /NO con. (%)
Ir/Al_2O_3	34.1	32.9	96
Ru/Al_2O_3	12.5	7.6	61
$Ir\text{-}Ru/Al_2O_3$	46.7	27.7	59

to previous reports, Ir metal can adsorb NO at atop, bridge, and hollow sites [70], of which the latter readily breaks the N—O bond, resulting in its dissociation into N and O atoms on the surface [50,69]. Thus, Ir/Al_2O_3 might possess a smaller amount of available hollow sites than Ru/Al_2O_3 and $Ir\text{-}Ru/Al_2O_3$. In addition, NO appeared to be adsorbed also at atop sites of all catalysts, as observed earlier in the DRIFT study (Fig. 5). For NO at the atop site, its direct dissociation may be less favorable than the indirect route involving its diffusion toward the hollow site followed by subsequent dissociation thereon [50]. A high diffusion barrier at atop sites might then be another reason for the low NO dissociation ability of Ir/Al_2O_3. Of course, the intrinsic reactivity of those sites may also depend on the electronic properties of metals themselves. Despite that the ratios of NO_{de}/NO_{con} of Ir-Ru/ and Ru/Al_2O_3 are similar, the area of consumed NO is significantly different. In detail, the area of consumed NO was 3.7 times higher in $Ir\text{-}Ru/Al_2O_3$ than in Ru/Al_2O_3. This difference might be due to the higher dispersion of active metals on $Ir\text{-}Ru/Al_2O_3$ (Table 1) and the change of the electronic and lattice structure caused by the formation of the Ir-Ru alloy.

The NO dissociation ability of the catalysts can also be evaluated indirectly by measuring the amount of N_2O generated during the adsorption step (Fig. S7), since the production of N_2O should be accompanied by cleavage of the N—O bond, followed by the subsequent reaction between the dissociated N atom and NO adsorbed [N* + NO* → N_2O(g)]. The amount of N_2O produced during the NO adsorption increases in the following order: Ir/Al_2O_3 < Ru/Al_2O_3 < < $Ir\text{-}Ru/Al_2O_3$. In particular, $Ir\text{-}Ru/Al_2O_3$ produces about 10 times more N_2O than Ir/Al_2O_3 does, indicating the extraordinary dissociation rate of NO. It should be noted that this N_2O formation must be suppressed in the presence of CO disturbing NO adsorption, as shown in Fig. 1(d). TPD experiments with the adsorption of 500 ppm NO and 5% O_2 simultaneously were also conducted to identify the effect of oxygen on the NO dissociation over the catalysts (Fig. S8). In contrast to the results of NO-TPD without oxygen, the amounts of NO consumed during the adsorption period are similar to those desorbed over both Ir-Ru/ and Ru/Al_2O_3 (NO_{de}/NO_{con} = 94 and 92 %, respectively), indicating their poor capability for NO decomposition in the presence of O_2. This indicates that the surface-adsorbed oxygen can interfere with the dissociation of NO. Based upon these TPD experiments, the Ir-Ru bimetallic catalyst has superior ability of breaking the N—O bond, and this feature can be one of the primary reasons for its high deNOx activity. However, how surface-covering oxygen is removed from Ir-Ru sites to effectively dissociate NO is still of importance.

3.5. Removal of surface-covering O

The NOx reduction process would also be limited by the reaction step involving removal of surface-covering O (reaction C.3) [71,72]. In fact, N and O atoms are chemisorbed on the catalyst surface via the NO dissociation step (reaction C.1), as discussed earlier. O atoms can still occupy the sites for NO dissociation even at temperature higher than 500 °C, resulting in self-poisoning, while the recombination of surface N readily occurs (reaction C.2) [51]. In addition, this residual O atom may withdraw electrons of metals, which reduces electron back-donation from the local d-band of metals to the 2p* antibonding orbital of NO. This in turn is unfavorable for the cleavage of the N—O bond [71,73]. Thus, removal of surface-covering O by CO is essential for reutilizing

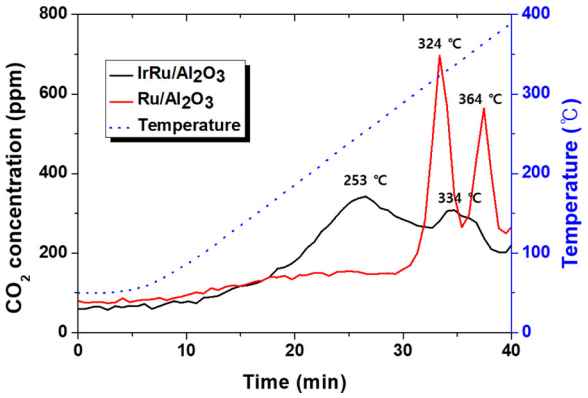

Fig. 8. Concentration of CO_2 generated by reaction between CO and oxygen dissociated from NO. Procedure: 1) NO adsorption (175 °C, 50 ppm NO/N_2, 1 h), 2) desorption (400 °C, N_2, 1 h), 3) CO-O reaction (50-400 °C, 0.7 % CO/N_2).

active sites.

As described earlier, $Ir\text{-}Ru/Al_2O_3$ showed the highest CO conversion among the catalysts employed under both standard and simple feed (CO-O_2) conditions (Figs. 1 and 2), indirectly indicating the high CO-O reactivity of the Ir-Ru alloy. However, to directly evaluate the reactivity of CO with the dissociated oxygen from NO over the catalysts, the following experiments were carried out. To produce surface oxygen on the metal, first NO was flowed into the pre-reduced catalysts at 175 °C. The catalyst surface would be covered mostly in the form of O* and NO*, and possibly N*, since NO was adsorbed both dissociatively and non-dissociatively at 175 °C, as described in the NO-TPD experiments (Fig. 7). After the NO adsorption period, the catalyst was purged with N_2 at 400 °C for 1 h to desorb the surface NO, while keeping surface-adsorbed oxygen. The temperature was determined on the basis of NO-TPD (Fig. 7) where NO is completely desorbed. Finally, the temperature was lowered to 50 °C and then 0.7 % CO/N_2 gas was flowed while heating up from 50 to 400 °C.

Fig. 8 presents concentrations of CO_2, generated by the reaction between CO and surface-covering O over the catalysts during the temperature ramp-up. CO_2 evolution over $Ir\text{-}Ru/Al_2O_3$ is gradually increased from 100 °C, the peaks of which are observed at 253 and 334 °C, respectively. The peak splitting may demonstrate the presence of at least two sites having different reactivity, which may be affected by either metal particle sizes or the support-metal interfacial interaction. In addition, two phases of Ir-Ru alloys, Ir-rich and Ru-rich analogues, might also contribute to this characteristic. Under the same experimental procedures, the Ru/Al_2O_3 catalyst has a first peak at 324 °C, which is about 70 °C higher than that of the $Ir\text{-}Ru/Al_2O_3$. This result indicates that the CO—O reactivity over $Ir\text{-}Ru/Al_2O_3$ is higher than that over Ru/Al_2O_3. The facile CO—O reaction over the Ir-Ru catalyst removes the surface oxygen dissociated from NO more rapidly, relieving the active site from being poisoned by oxygen, which is beneficial for the successive NO dissociation required for the NOx removal. The lower reactivity of surface oxygen on Ru/Al_2O_3 with CO may be due to the higher oxygen affinity of Ru metal than other platinum group metal counterparts [27], which appeared to be moderated by the partial substitution of Ru atoms with Ir, as discussed earlier.

The effect of O_2 affinity on the deNOx activity has become more pronounced over each catalyst, when O_2 is directly added in the feed stream. Comparing Fig. 1(a) with Fig. 2(a), oxygen drastically lowered the lean deNOx performance of the Ru/Al_2O_3 catalyst, while it reversed in the case of the Ir-Ru bimetallic counterpart. To directly investigate the effect of O_2 poisoning on the catalytic behavior in detail, an activity test was further carried out by varying the feed condition while maintaining the reaction temperature at 175 °C. The first two steps in Fig. 9(a) show the response of NO conversion to the O_2 addition in the

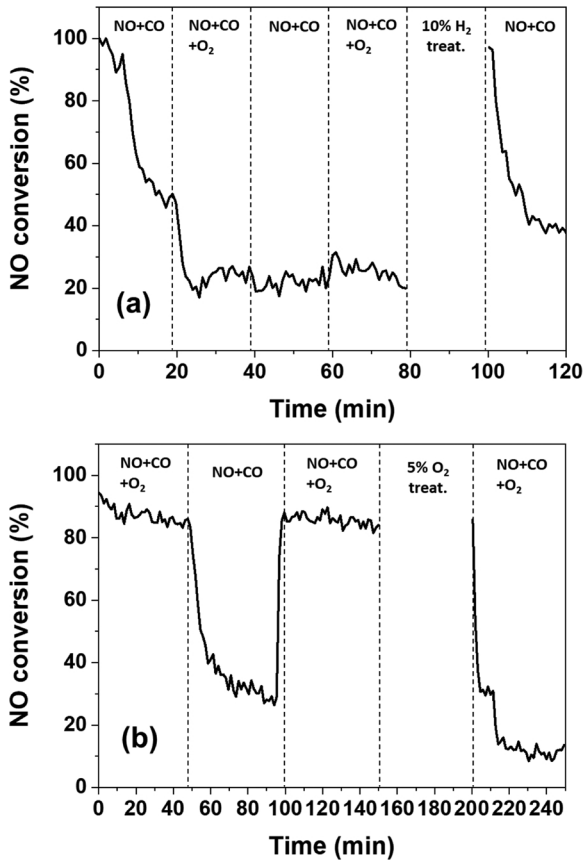

Fig. 9. The response of NO conversion to the various feed conditions (50 ppm NO, 0.7 % CO, 5% O_2 and N_2 balance) at 175 °C: (a) Ru/Al_2O_3, (b) $Ir\text{-}Ru/Al_2O_3$.

feed stream (NO−CO) over Ru/Al_2O_3. NO conversion of Ru/Al_2O_3 dropped sharply as soon as O_2 was added, and it was not recovered even though O_2 addition was stopped. However, after the H_2 treatment (10 % H_2/N_2, 50 min), the catalytic activity was restored to the initial level. This indicates that the Ru site was poisoned by oxygen during the deNOx reaction, and once poisoned, NOx reduction by CO could not proceed. The poisoning of O_2 appeared to be removed by flowing hydrogen at this temperature. As discussed before, Ru-based catalysts are known to have poor O tolerance for lean NOx reduction by CO. Parvulescu et al. described that, although Ru catalyst showed higher activity in the reduction of NO with CO than other noble metal-based analogues (Pt, Pd and Rh), small amounts of O_2 addition were largely detrimental to its deNOx activity [74]. Recently, a similar result was reported by Bartley et al. [75]. They showed that the Ru-based catalyst can reduce NOx to N_2 with 100 % efficiency in O_2-deficient conditions, but no activity was observed in the O_2–rich condition, consistent with our results. As discussed before, Ru-based catalysts are known to have superior O_2 affinity to other noble metal-based counterparts. Again, as the surface oxygen coverage increases, the electron density nearby metals would decrease, which reduces the degree of π back-bonding from the local d-band of metals to the 2p* antibonding orbital of NO, resulting in a higher activation barrier for the NO dissociation [71,73]. In addition, this reaction step would also be affected by the catalyst support, particularly in the presence of strong metal support interaction (SMSI) inducing electron donation or withdrawal from the support to Ir-Ru alloy. Further studies are necessary to clearly understand the support effect.

On the other hand, the $Ir\text{-}Ru/Al_2O_3$ catalyst shows high and stable NO conversion albeit O_2 presence (Fig. 9(b)), indicating superior O_2 tolerance of $Ir\text{-}Ru/Al_2O_3$. After O_2 was excluded from the feed stream, the NO conversion was significantly reduced, opposite to the case with Ru/Al_2O_3. This decline of the NO conversion can be explained by the inhibiting effect of CO on metal sites. Indeed, Ir metal is known to be easily poisoned by CO due to its high adsorption affinity with CO [33]. Once O_2 is added again to the feed stream, the NOx removal performance of the $Ir\text{-}Ru/Al_2O_3$ catalyst is immediately recovered to the initial state. This indicates that the CO-induced decline in deNOx activity is reversible, capable of being restored by the consumption of CO via oxidation. The inhibiting effect of CO on the deNOx activity can also be determined by the NO−CO reaction over $Ir\text{-}Ru/Al_2O_3$ with respect to the inlet concentration of CO. Lowering the CO concentration from 7000 to 600 ppm turned out to enhance NO conversion of $Ir\text{-}Ru/Al_2O_3$ from 38 to 80 %, demonstrating that CO, which is supposed to be involved in the NOx reduction, can also interrupt the reaction cycle at the low temperature (Fig. S9). The deNOx activity of Ru/Al_2O_3 is not significantly dependent upon the CO concentration, which might be attributed to its CO adsorption property, different from $Ir\text{-}Ru/Al_2O_3$. Further studies on this CO inhibiting effect are in progress with both experimental and computational approaches.

The superior O_2 tolerance of $Ir\text{-}Ru/Al_2O_3$ can be interpreted in two respects: (1) the inherent O_2 resistance of the Ir-Ru site and (2) fast removal of poisoning oxygen by CO-O reaction. To determine the intrinsic resistance of the Ir-Ru catalyst toward O_2, the catalytic performance was examined again after exposure to O_2 without NO and CO (Fig. 9(b)). After treatment in 5% O_2 in N_2 for 50 min, no catalytic activity was observed over $Ir\text{-}Ru/Al_2O_3$, indicating that this catalyst might not be fully free of O_2 poisoning. We can thus conclude that the superior O_2 tolerance of $Ir\text{-}Ru/Al_2O_3$ can be attributed mainly to the fast CO-O reaction, which is able to immediately remove the poisoning oxygen on the surface. This high reactivity of the Ir-Ru catalyst may also be reflected in the DRIFTs results (Fig. 6). As shown in Fig. 6(d), the peak of 1780 cm^{-1} was clearly observed even in NO + CO + O_2 flow attributed to NO adsorbed on the oxygen free surface, which means that the chemisorbed oxygen can be removed by CO sufficiently over the Ir-Ru catalyst under the lean deNOx condition, required for the successive NO decomposition. As a result, the facile CO-O reaction of $Ir\text{-}Ru/Al_2O_3$ can alleviate the inhibiting effect of CO and O_2 simultaneously, thereby enhancing the lean NOx reduction performance by CO significantly.

Based upon the experimental results, NO dissociation ability and CO reactivity with surface oxygen, required for the high deNOx activity under the lean condition, have been investigated over the catalysts employed. However, it was difficult to directly evaluate reaction steps regarding N_2 formation by experimental studies (reactions C.2 & C.4). Computational calculations have thus been performed using density functional theory (DFT) to resolve this difficulty, and further to ensure our experimental data are reliable, as will be described in the following section.

3.6. Reaction energetics

The above-mentioned experimental observations are the results of comprehensive reflections of microscopic effects such as surface structure, number of active sites, metal particle size, etc. To identify the intrinsic reaction energetics of a catalytic material, we performed a series of DFT calculations for catalysis on ideal surfaces of the Ir, Ru, and Ir-Ru alloy. For the alloy model, we chose L12 alloy structure where 1/4 Ir atoms in their own lattice were replaced with Ru, resulting in Ir3Ru1 composition. This is based on the XRD observations (Fig. 3), which suggested the fcc-like crystal structure of the IrRu alloy. According to the suggestion from experiments, four individual reactions, NO dissociation, CO oxidation, N–N recombination, and NO disproportionation, were considered to have a major effect on the catalytic performance (Fig. 10). We note that the addition of H_2O can also largely affect the reaction energetics but such effect is not considered in the present study. As shown in Fig. S2 in the Supplementary Material, the H_2O supplied with the reactants appeared to be adsorbed

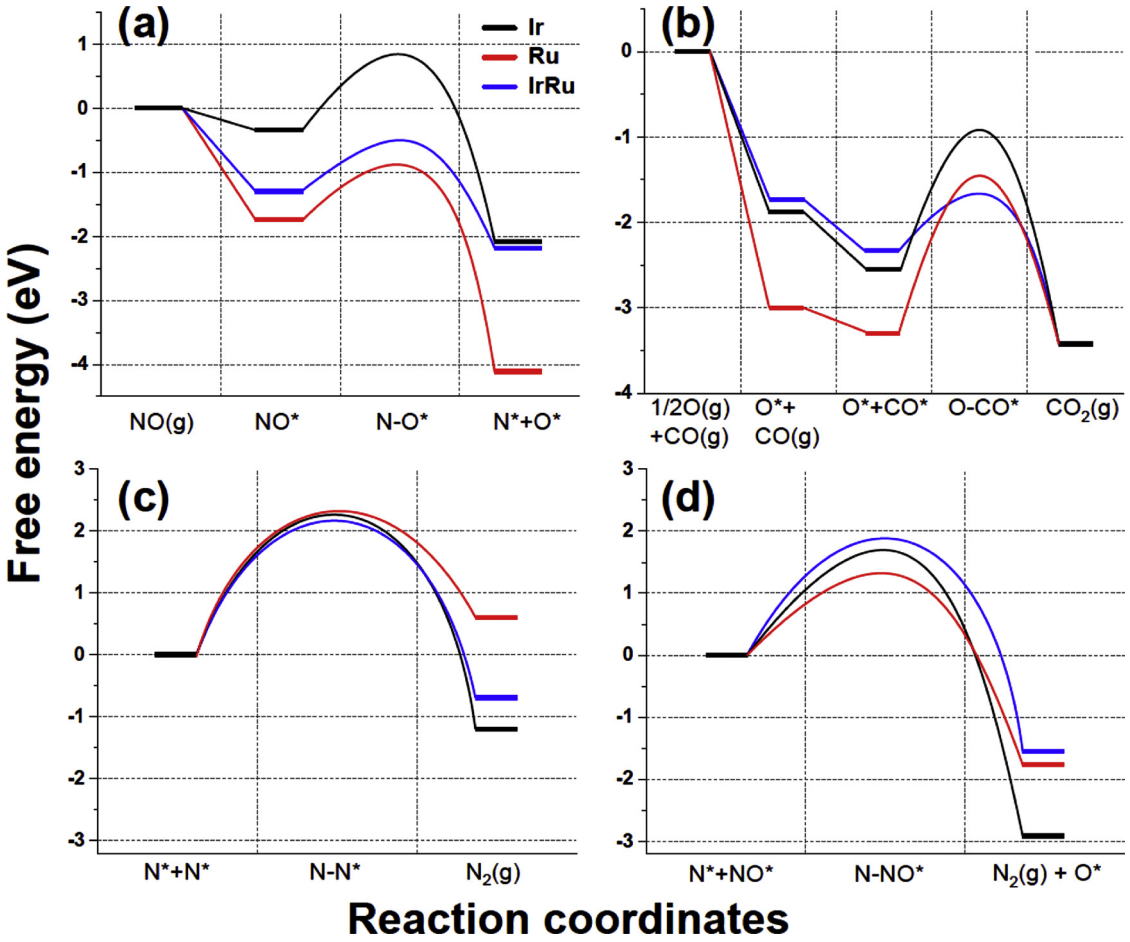

Fig. 10. Free energies of four individual surface reactions. (a) NO dissociation, (b) CO oxidation, (c) N–N recombination, and (d) NO disproportionation. Free energies were calculated assuming reaction condition of T = 175 °C and P = 0.1 MPa., and * denote the gas-phase and surface-bound species, respectively.

preferentially on the hydrophilic Al_2O_3 support rather than on the metallic surface based on the marginal performance changes by the H_2O addition.

Fig. 10(a) shows that the NO dissociations on all three metal surfaces are favored showing exergonic energetics, but Ir shows a larger kinetic barrier (1.18 eV) than Ru (0.86 eV) and Ir-Ru alloy (0.80 eV), suggesting its slow NO dissociation. The relative low NO dissociation ability of Ir is in accordance with the results of NO−CO reaction (Fig. 2(a)) and NO-TPD (Fig. 7). Ru exhibits most advantageous NO dissociation energetics among surfaces calculated due to its strong interaction with oxygen. However, its activation barrier is comparable with that of the Ir-Ru alloy, supporting similar NO−CO reaction performances for both catalysts.

The DFT results also demonstrate that the Ir-Ru alloy is more advantageous for the removal of surface-bound O and CO by forming CO_2 than the Ir and Ru surfaces (Fig. 10(b)). The Ir-Ru alloy shows much smaller activation barrier for the CO oxidation (0.66 eV) than Ir (1.64) and Ru (1.84) surfaces. Experimental results (Fig. 2(b) and Fig. 8) are well correlated with this theoretical elucidation, showing a rapid CO oxidation rate on the Ir-Ru catalysts. The oxygen tolerance tests (Fig. 9) indicated that the Ru catalyst was vulnerable to the surface oxidation, which was not easily reduced by CO. The DFT calculations explain this phenomenon by overly strong adsorption of O and CO on the Ru surface, which occupy active sites and hinder the subsequent surface reactions. In the case of Ir, the adsorptions of CO and O are not such strong but its high activation barrier make the reaction slow as in Fig. 2(b).

In addition to the O* removal, another reaction that maintains the number of active sites is N* removal by forming N_2. Two possible pathways, N–N recombination and NO disproportionation, are considered in the present study. For three catalyst surfaces, the NO disproportionation is calculated to be slightly more favorable than the N–N recombination. The activation barriers for the NO disproportionation are ranged between 1.32 and 1.91 eV, while those of the N–N recombination are ranged between 2.17 and 2.30 eV. The two paths will be competitive in realistic condition because the energy differences are not significant but, this reminds the importance of the surface oxygen removal because the surface oxygen is also produced even in the N_2 formation step.

Based upon the obtained experimental and calculated results, the excellent deNOx activity of the Ir-Ru bimetallic catalyst may be understood as shown in Fig. 11. NOx reduction by CO over all catalysts employed is likely to proceed via the “NO dissociative model” without involving reaction intermediates induced by CO such as NCO. NO is first dissociated into N and O atoms readily on Ir-Ru alloys (reaction C.1), while the Ir monometallic phase turned out to be much less efficient for breaking the N−O bond. The surface-covering oxygen atom can give rise to “self-poisoning” interrupting successive NO decomposition, which would be effectively alleviated over Ir-Ru/Al_2O_3 by the facile CO−O surface reaction (reaction C.3). This catalytic property of the Ir-Ru bimetallic catalyst appeared to be highly beneficial for the NOx reduction in the presence of O_2, whereas Ru/Al_2O_3 having strong affinity toward O_2 was nearly inactive under the condition by O_2 poisoning. It is also noteworthy that various in-depth studies, such as the influence of the support and the identification of active sites, are required to understand the promotional effect of the Ir-Ru catalyst proposed in the present study.

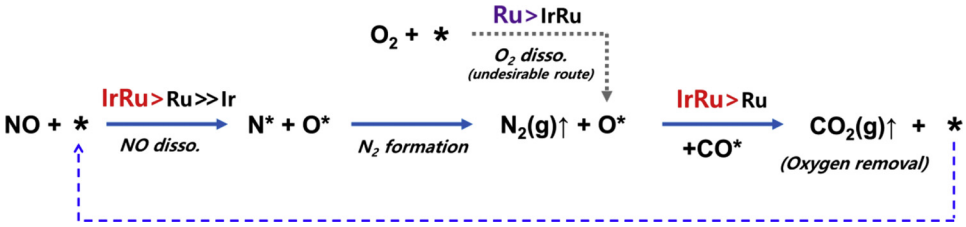

Fig. 11. High-efficiency reaction cycle for reducing NOx over Ir-Ru/Al_2O_3.

4. Conclusion

Ir-Ru/Al_2O_3 has been systematically compared to those of monometallic catalysts, Ir/ and Ru/Al_2O_3, in terms of catalytic activity and properties for lean NOx reduction by CO to unravel the origin of the synergistic effect between Ir and Ru. Ir-Ru/Al_2O_3 showed superior NOx reduction activity by CO under lean conditions, compared to the monometallic catalysts. NOx conversion of 91 % was achieved over Ir-Ru/Al_2O_3 at 175 ˚C, while the Ir and Ru monometallic catalysts have no deNOx activity at the identical temperature. The Ir-Ru alloy appeared to be the main phases in Ir-Ru/Al_2O_3, as confirmed by XRD and EXAFS measurements. The formation of this alloy structure was likely to result in alterations of the adsorption property and the surface chemistry of reactants on each catalyst. DRIFTs results demonstrated that the lean NOx reduction by CO over all catalysts employed may proceed via the "NO dissociative model". The NO-TPD results revealed that NO could be effectively dissociated on the Ir-Ru alloy and Ru monometallic sites at 175 ˚C, whereas it was mostly adsorbed molecularly on Ir site without its dissociation. Although the Ru monometallic catalyst showed comparable NO−CO reactivity to Ir-Ru/Al_2O_3, the deNOx performance was greatly decreased when O_2 was added, possibly due to O_2 poisoning, opposite to the bimetallic catalyst. The CO-O surface reactivity turned out to be higher over the Ir-Ru catalyst than over the Ru catalyst. This is highly beneficial for the removal of poisoning CO and oxygen dissociated from NO/O_2 on the catalyst surface, allowing the active sites to dissociate NO continuously.

DFT calculations also demonstrated consistent results with experimental data revealing that the Ir-Ru alloy has desirable energetics for NO dissociation and CO*-O* reactions, whereas Ir and Ru surfaces are less favorable for the former and latter steps, respectively. In addition, DFT results indicated that N_2 formation may occur more easily through NO disproportionation reaction than the N–N recombination pathway, the rate of which may not significantly vary with the metal types employed.

Consequently, the Ir-Ru catalyst may effectively dissociate NO into N* and O* on the alloy phase even at low temperature, and then produce N_2 predominately by NO* + N* reaction, while this active site is successively reutilized by the facile CO-O reaction, which is believed to be the primary cause of its high NOx reduction activity.

CRediT authorship contribution statement

Young-Woo You: Investigation, Writing - original draft. **Young Jin Kim:** Investigation, Writing - original draft. **Jin Hee Lee:** Investigation, Resources. **Malik Waqar Arshad:** Investigation, Resources. **Seok Ki Kim:** Investigation, Resources. **Soo Min Kim:** Investigation, Resources. **Hyunjoo Lee:** Validation. **Levi T. Thompson:** Validation. **Iljeong Heo:** Supervision, Writing - review & editing.

Declaration of Competing Interest

The authors declare that they have no known competing financial interests or personal relationships that could have appeared to influence the work reported in this paper.

Acknowledgements

The authors would like to thank all staff involving automotive catalysis at POSTECH, KIMM, Seoul National University, University of Michigan, GM R&D, HMC R&D for helpful discussions. This work was supported by Institutional Research Program of KRICT (SI2061-22) and KIST (IP20-07, 2E30860-20-P052, "Atmospheric Environment Research Program"). The experiments at PLS were supported in part by MSIP and POSTECH. This research was also supported by the Technology Development Program to Solve Climate Changes through the National Research Foundation of Korea (NRF) funded by the Ministry of Science, ICT (NRF-2019M1A2A2103855).

Appendix A. Supplementary data

Supplementary material related to this article can be found, in the online version, at doi:https://doi.org/10.1016/j.apcatb.2020.119374.

References

[1] European Environment Agency, Average CO_2 Emissions from Newly Registered Motor Vehicles, (2019).
[2] Y.J. Kim, J.K. Lee, K.M. Min, S.B. Hong, I.-S. Nam, B.K. Cho, Hydrothermal stability of CuSSZ13 for reducing NOx by NH_3, J. Catal. 311 (2014) 447–457.
[3] J. Kašpar, P. Fornasiero, N. Hickey, Automotive catalytic converters: current status and some perspectives, Catal. Today 77 (2003) 419–449.
[4] I.A. Resitoglu, A. Keskin, Hydrogen applications in selective catalytic reduction of NOx emissions from diesel engines, Int. J. Hydrogen Energy 42 (2017) 23389–23394.
[5] X. Wang, W. Wen, J. Mi, X. Li, R. Wang, The ordered mesoporous transition metal oxides for selective catalytic reduction of NOx at low temperature, Appl. Catal. B 176–177 (2015) 454–463.
[6] J.P. Breen, R. Burch, A review of the effect of the addition of hydrogen in the selective catalytic reduction of NOx with hydrocarbons on silver catalysts, Top. Catal. 39 (2006) 53–58.
[7] H. Hamada, M. Haneda, A review of selective catalytic reduction of nitrogen oxides with hydrogen and carbon monoxide, Appl. Catal. A Gen. 421–422 (2012) 1–13.
[8] I. Heo, S. Sung, M.B. Park, T.S. Chang, Y.J. Kim, B.K. Cho, S.B. Hong, J.W. Choung, I.-S. Nam, Effect of hydrocarbon on DeNOx performance of selective catalytic reduction by a combined reductant over Cu-containing zeolite catalysts, ACS Catal. 9 (2019) 9800–9812.
[9] L. Xu, R.W. McCabe, LNT + in situ SCR catalyst system for diesel emissions control, Catal. Today 184 (2012) 83–94.
[10] I. Heo, M.K. Kim, S. Sung, I.S. Nam, B.K. Cho, K.L. Olson, W. Li, Combination of photocatalysis and HC/SCR for improved activity and durability of DeNOx catalysts, Environ. Sci. Technol. 47 (2013) 3657–3664.
[11] D.B. Nguyen, V.T. Nguyen, I.J. Heo, Y.S. Mok, Removal of NOx by selective catalytic reduction coupled with plasma under temperature fluctuation condition, J. Ind. Eng. Chem. 72 (2019) 400–407.
[12] J.E. Dec, Advanced compression-ignition engines—understanding the in-cylinder processes, Proc. Combust. Inst. 32 (2009) 2727–2742.
[13] E. Shim, H. Park, C. Bae, Comparisons of advanced combustion technologies (HCCI, PCCI, and dual-fuel PCCI) on engine performance and emission characteristics in a heavy-duty diesel engine, Fuel 262 (2020).
[14] D. Lopes, F. Zotin, L.A. Palacio, Copper-nickel catalysts from hydrotalcite precursors: the performance in NO reduction by CO, Appl. Catal. B 237 (2018) 327–338.
[15] X. Cheng, X. Zhang, D. Su, Z. Wang, J. Chang, C. Ma, NO reduction by CO over copper catalyst supported on mixed CeO_2 and Fe_2O_3: catalyst design and activity test, Appl. Catal. B 239 (2018) 485–501.
[16] L. Wang, X. Cheng, Z. Wang, C. Ma, Y. Qin, Investigation on Fe-Co binary metal oxides supported on activated semi-coke for NO reduction by CO, Appl. Catal. B 201 (2017) 636–651.
[17] M. Haneda, T. Yoshinari, K. Sato, Y. Kintaichi, H. Hamada, Ir/SiO_2 as a highly active catalyst for the selective reduction of NO with CO in the presence of O_2 and SO_2, Chem. Commun. (2003) 2814–2815.
[18] A. Wang, Unique properties of Ir/ZSM-5 catalyst for NO reduction with CO in the

presence of excess oxygen, Appl. Catal. B 40 (2003) 319–329.
[19] A. Takahashi, I. Nakamura, M. Haneda, T. Fujitani, H. Hamada, Role of tungsten in promoting selective reduction of NO with CO over $Ir/WO_3–SiO_2$ catalysts, Catal. Lett. 112 (2006) 133–138.
[20] M. Haneda, H. Kudo, Y. Nagao, T. Fujitani, H. Hamada, Enhanced activity of Ba-doped Ir/SiO2 catalyst for NO reduction with CO in the presence of O_2 and SO_2, Catal. Commun. 7 (2006) 423–426.
[21] Y.J. Kim, H.J. Kwon, I. Heo, I.-S. Nam, B.K. Cho, J.W. Choung, M.-S. Cha, G.K. Yeo, Mn–Fe/ZSM5 as a low-temperature SCR catalyst to remove NOx from diesel engine exhaust, Appl. Catal. B 126 (2012) 9–21.
[22] I. Heo, J.R. Gaudet, S.J. Schmieg, C.H. Kim, L.T. Thompson, Supported platinum group metals for low temperature CO selective catalytic reduction, 24th North American Catalysis Society Meeting, Pittsburgh PA 2015 June, 2015.
[23] J.H. Song, D.C. Park, Y.-W. You, T.S. Chang, I. Heo, D.H. Kim, Lean NOx reduction by CO at low temperature over bimetallic $IrRu/Al_2O_3$ catalysts with different Ir : Ru ratios, Catal. Sci. Technol. 10 (2020) 2120–2136.
[24] I. Heo, Y.W. You, J.H. Lee, S.J. Schmieg, D.Y. Yoon, C.H. Kim, Urealess NOx reduction by carbon monoxide in simulated lean-burn exhausts, Environ. Sci. Technol. 54 (2020) 8344–8351.
[25] K. Lee, É.D. Murray, L. Kong, B.I. Lundqvist, D.C. Langreth, Higher-accuracy van der Waals density functional, Phys. Rev., B Condens. Matter 82 (2010).
[26] S. Kim, G. Park, M.H. Woo, G. Kwak, S.K. Kim, Control of hierarchical structure and Framework-Al distribution of ZSM-5 via adjusting crystallization temperature and their effects on methanol conversion, ACS Catal. 9 (2019) 2880–2892.
[27] D.W. Goodman, C.H.F. Peden, M.S. Chen, CO oxidation on ruthenium: the nature of the active catalytic surface, Surf. Sci. 601 (2007) L124–L126.
[28] R.L. Martins, M.A.S. Baldanza, M. Schmal, An infrared study of NO and CO adsorption on zeolite-supported Ru and Ru − Pt catalysts, J. Phys. Chem. B 105 (2001) 10303–10307.
[29] G. BrodÉn, T.N. Rhodin, C. Brucker, R. Benbow, Z. Hurych, Synchrotron radiation study of chemisorptive bonding of CO on transition metals — polarization effect on Ir(100), Surf. Sci. 59 (1976) 593–611.
[30] A. Hornung, M. Muhler, G. Ertl, On the mechanism of the selective catalytic reduction of NO to N_2 by H_2 over Ru/MgO and Ru/Al_2O_3 catalysts, Top. Catal. 11 (2000) 263–270.
[31] K. Qadir, S.H. Joo, B.S. Mun, D.R. Butcher, J.R. Renzas, F. Aksoy, Z. Liu, G.A. Somorjai, J.Y. Park, Intrinsic relation between catalytic activity of CO oxidation on Ru nanoparticles and Ru oxides uncovered with ambient pressure XPS, Nano Lett. 12 (2012) 5761–5768.
[32] N.W. Cant, P.C. Hicks, B.S. Lennon, Steady-state oxidation of carbon monoxide over supported noble metals with particular reference to platinum, J. Catal. 54 (1978) 372–383.
[33] K. Ueda, M. Yoshida, K. Isegawa, N. Shirahata, K. Amemiya, K. Mase, B.S. Mun, H. Kondoh, Operando observation of NO reduction by CO on Ir(111) surface using NAP-XPS and mass spectrometry: dominant reaction pathway to N2 formation under near realistic conditions, J. Phys. Chem. C 121 (2017) 1763–1769.
[34] A.S. Wörz, K. Judai, S. Abbet, U. Heiz, Cluster size-dependent mechanisms of the CO + NO reaction on small pdn (n ≤ 30) clusters on oxide surfaces, J. Am. Chem. Soc. 125 (2003) 7964–7970.
[35] H. Wang, H.D. Abruna, IrPdRu/C as H2 oxidation catalysts for alkaline fuel cells, J. Am. Chem. Soc. 139 (2017) 6807–6810.
[36] J. Ohyama, D. Kumada, A. Satsuma, Improved hydrogen oxidation reaction under alkaline conditions by ruthenium–iridium alloyed nanoparticles, J. Mater. Chem. A 4 (2016) 15980–15985.
[37] H. Okamoto, The Ir-Ru (iridium-ruthenium) system, J. Phase Equilibria Diffus. 13 (1992) 565–567.
[38] W. Du, N.A. Deskins, D. Su, X. Teng, Iridium–ruthenium alloyed nanoparticles for the ethanol oxidation fuel cell reactions, ACS Catal. 2 (2012) 1226–1231.
[39] H. Hamada, M.G. Samant, M. Boudart, X-ray absorption spectroscopy of silica-supported Ir–Ru bimetallic clusters, Chem. Lett. 15 (1986) 885–888.
[40] S. Smeekens, S. Heylen, K. Villani, K. Houthoofd, E. Godard, M. Tromp, J.W. Seo, M. DeMarco, C.E.A. Kirschhock, J.A. Martens, Reversible NOx storage over Ru/Na–Y zeolite, Chem. Sci. 1 (2010).
[41] C.R. O'Connor, M.A. van Spronsen, T. Egle, F. Xu, H.R. Kersell, J. Oliver-Meseguer, M. Karatok, M. Salmeron, R.J. Madix, C.M. Friend, Hydrogen migration at restructuring palladium-silver oxide boundaries dramatically enhances reduction rate of silver oxide, Nat. Commun. 11 (2020) 1844.
[42] J. Courtois, W. Du, E. Wong, X. Teng, N.A. Deskins, Screening iridium-based bimetallic alloys as catalysts for direct ethanol fuel cells, Appl. Catal. A Gen. 483 (2014) 85–96.
[43] N. Danilovic, R. Subbaraman, K.C. Chang, S.H. Chang, Y. Kang, J. Snyder, A.P. Paulikas, D. Strmcnik, Y.T. Kim, D. Myers, V.R. Stamenkovic, N.M. Markovic, Using surface segregation to design stable Ru-Ir oxides for the oxygen evolution reaction in acidic environments, Angew. Chem. Int. Ed. 53 (2014) 14016–14021.
[44] A.A. Davydov, A.T. Bell, An infrared study of NO and CO adsorption on a silica-supported Ru catalyst, J. Catal. 49 (1977) 332–344.
[45] M.F. Brown, R.D. Gonzalez, An infrared study of the interaction between adsorbed CO and adsorbed NO on supported Ru and supported Pt, J. Catal. 44 (1976) 477–487.
[46] K. Almusaiteer, S.S.C. Chuang, Isolation of active adsorbates for the NO-CO reaction on Pd/Al_2O_3 by selective enhancement and selective poisoning, J. Catal. 180 (1998) 161–170.
[47] H. Jeong, G. Lee, B.S. Kim, J. Bae, J.W. Han, H. Lee, Fully dispersed Rh ensemble catalyst to enhance low-temperature activity, J. Am. Chem. Soc. 140 (2018) 9558–9565.
[48] V.G. Komvokis, G.E. Marnellos, I.A. Vasalos, K.S. Triantafyllidis, Effect of pre-treatment and regeneration conditions of $Ru/\gamma\text{-}Al_2O_3$ catalysts for N_2O decomposition and/or reduction in O_2-rich atmospheres and in the presence of NOx, SO_2 and H_2O, Appl. Catal. B 89 (2009) 627–634.
[49] J.M. González-Carballo, F.J. Pérez-Alonso, F.J. García-García, M. Ojeda, J.L.G. Fierro, S. Rojas, In-situ study of the promotional effect of chlorine on the Fischer–Tropsch synthesis with Ru/Al2O3, J. Catal. 332 (2015) 177–186.
[50] C.Z. He, H. Wang, P. Zhu, J.Y. Liu, Adsorption and dissociation of NO on Ir(100): a first-principles study, J. Chem. Phys. 135 (2011) 204707.
[51] W. Chen, T.E. Madey, A.L. Stottlemyer, J.G. Chen, P. Kaghazchi, T. Jacob, Structure sensitivity in adsorption and decomposition of NO on Ir, J. Phys. Chem. C 112 (2008) 19113–19120.
[52] C. Elmasides, D.I. Kondarides, W. Grünert, X.E. Verykios, XPS and FTIR study of Ru/Al_2O_3 and Ru/TiO_2 catalysts: reduction characteristics and interaction with a methane − oxygen mixture, J. Phys. Chem. B 103 (1999) 5227–5239.
[53] L. Li, F. Zhang, N. Guan, M. Richter, R. Fricke, Selective catalytic reduction of NO by propane in excess oxygen over IrCu-ZSM-5 catalyst, Catal. Commun. 8 (2007) 583–588.
[54] T. Boningari, S.M. Pavani, P.R. Ettireddy, S.S.C. Chuang, P.G. Smirniotis, Mechanistic investigations on NO reduction with CO over Mn/TiO_2 catalyst at low temperatures, Mol. Catal. 451 (2018) 33–42.
[55] E. Guglielminotti, F. Boccuzzi, Infrared spectroscopic study of ammonia and nitric oxide adsorption and reactivity on a Ru/TiO_2 catalyst: effect of oxo-reducing treatments, J. Chem. Soc. Faraday Trans. 87 (1991) 337–343.
[56] M. Nawdali, E. Iojoiu, P. Gélin, H. Praliaud, M. Primet, Influence of the pre-treatment on the structure and reactivity of $Ir/\gamma\text{-}Al_2O_3$ catalysts in the selective reduction of nitric oxide by propene, Appl. Catal. A 220 (2001) 129–139.
[57] J. Szanyi, J. Hun Kwak, R.A. Moline, C.H.F. Peden, The adsorption of NO_2 and the NO + O_2 reaction on Na-Y,FAU: an in situ FTIR investigation, PCCP 5 (2003) 4045–4051.
[58] C. Tang, S. Zou, M.W. Severson, M.J. Weaver, Infrared spectroscopy of mixed nitric-oxide − carbon-monoxide adlayers on ordered iridium(111) in aqueous solution: a model study of coadsorbate vibrational interactions, J. Phys. Chem. B 102 (1998) 8546–8556.
[59] L. Tan, L. Huang, Y. Liu, Q. Wang, Detailed mechanism of the NO + CO reaction on Rh(1 0 0) and Rh(1 1 1): a first-principles study, Appl. Surf. Sci. 444 (2018) 276–286.
[60] M.L. Unland, Isocyanate intermediates in the reaction of NO and CO over noble metal catalysts, J. Catal. 31 (1973) 459–465.
[61] T. Fujitani, I. Nakamura, A. Takahashi, M. Haneda, H. Hamada, Kinetics and mechanism of NO reduction with CO on Ir surfaces, J. Catal. 253 (2008) 139–147.
[62] P. Granger, C. Dathy, J.J. Lecomte, L. Leclercq, M. Prigent, G. Mabilon, G. Leclercq, Kinetics of the NO and CO reaction over platinum catalysts: I. Influence of the support, J. Catal. 173 (1998) 304–314.
[63] P. Xiao, R.C. Davis, X. Ouyang, J. Li, A. Thomas, S.L. Scott, J. Zhu, Mechanism of NO reduction by CO over Pt/SBA-15, Catal. Commun. 50 (2014) 69–72.
[64] W. Chen, Q. Shen, R.A. Bartynski, P. Kaghazchi, T. Jacob, Reduction of NO by CO on unsupported Ir: bridging the materials gap, ChemPhysChem 11 (2010) 2515–2520.
[65] S. Zhang, Y. Tang, L. Nguyen, Y.-F. Zhao, Z. Wu, T.-W. Goh, J.J. Liu, Y. Li, T. Zhu, W. Huang, A.I. Frenkel, J. Li, F.F. Tao, Catalysis on singly dispersed Rh atoms anchored on an inert support, ACS Catal. 8 (2017) 110–121.
[66] M. Kantcheva, O. Samarskaya, L. Ilieva, G. Pantaleo, A.M. Venezia, D. Andreeva, In situ FT-IR investigation of the reduction of NO with CO over $Au/CeO_2\text{-}Al_2O_3$ catalyst in the presence and absence of H_2, Appl. Catal. B 88 (2009) 113–126.
[67] A. Shichi, T. Hattori, A. Satsuma, Involvement of NCO species in promotion effect of water vapor on propane-SCR over Co-MFI zeolite, Appl. Catal. B 77 (2007) 92–99.
[68] S.-K. Park, Y.-K. Park, S.-E. Park, L. Kevan, Comparison of selective catalytic reduction of NO with C_3H_6 and C_3H_8 over Cu(II)-ZSM-5 and Co(II)-ZSM-5, PCCP 2 (2000) 5500–5509.
[69] I. Nakamura, T. Fujitani, Adsorption behavior and reaction properties of NO and CO on Ir(111) and Rh(111), Catal. Surv. from Asia 13 (2009) 22–29.
[70] I.A. Erikat, B.A. Hamad, J.M. Khalifeh, A density functional study for adsorption and oxidation of NO on Ir (100) surface, Appl. Catal. A 449 (2012) 9–14.
[71] W. Chen, A.L. Stottlemyer, J.G. Chen, P. Kaghazchi, T. Jacob, T.E. Madey, R.A. Bartynski, Adsorption and decomposition of NO on O-covered planar and faceted Ir(210), Surf. Sci. 603 (2009) 3136–3144.
[72] C. Wögerbauer, M. Maciejewski, M.M. Schubert, A. Baiker, Effect of sodium on the catalytic properties of iridium black in the selective reduction of NOx by propene under lean-burn conditions, Catal. Lett. 74 (2001) 1–7.
[73] M.D. Amiridis, C. Mihut, M. Maciejewski, A. Baiker, The selective catalytic reduction of NO by hydrocarbons over Pt- and Ir-based catalysts, Top. Catal. 28 (2004) 141–150.
[74] V.I. Pârvulescu, P. Grange, B. Delmon, Catalytic removal of NO, Catal. Today 46 (1998) 233–316.
[75] G.J. Bartley, Z. Tonzetich, R. Hartley, Ruthenium-Based Catalyst in EGR Leg of a D-EGR Engine Offers Combustion Improvements Through Selective NOX Removal, SAE Tech., 2016.